Available online at www.sciencedirect.com

SciVerse ScienceDirect

Ceramics International 39 (2013) 5335–5341

CERAMICS INTERNATIONAL

www.elsevier.com/locate/ceramint

The influence of reactive milling on the structure and magnetic properties of nanocrystalline $MnFe_2O_4$

Sadan Ozcan*, Serkan Akansel, Abdullah Ceylan

Physics Engineering Department, Hacettepe University, Beytepe, Ankara 06800, TURKEY

Received 27 November 2012; received in revised form 10 December 2012; accepted 11 December 2012
Available online 11 January 2013

Abstract

Nanocrystalline manganese ferrites ($MnFe_2O_4$) have been synthesized by direct milling of metallic manganese (Mn) and iron (Fe) powders in distilled water (H_2O). In order to overcome the limitation of wet milling, dry milling procedure has also been utilized to reduce crystallite size. The effects of milling time on the formation and crystallite size of wet milled $MnFe_2O_4$ nanoparticles have been investigated. It has been observed that single phase 18.4 nm nanocrystalline $MnFe_2O_4$ is obtained after 24 h milling at 400 rpm. Further milling caused deformation of the structure as well as increased crystallite size. With the aim of reducing the crystallite size of 18.4 nm, $MnFe_2O_4$ sample dry milling has been implemented for 2 and 4 h at 300 rpm. As a result, the crystallite size has been reduced to 12.4 and 8.7 nm, respectively. Effects of the crystalline sizes on magnetic properties were also investigated. Magnetization results clearly demonstrated that crystallite size has much more effect on the magnetic properties than average particle size.

Keywords: A. Milling; C. Magnetic properties; D. Ferrites; Mechanochemistry

1. Introduction

Materials with sizes on the order of 10–100 nm are called nanocrystallites [1–5]. In general, crystallite size often matches with grain size but there are exceptions. Depending on the synthesis technique, nanoparticles might possess one or more nanocrystallites. Therefore, nanocrystallite structures are composed of the large number of atoms residing around grain boundaries as compared to course grained polycrystalline counterparts [1–3]. As such it is expected that these interfaces give rise to pronounced changes to the chemical, physical, optical and magnetic properties.

Among all the nanomaterial preparation methods, mechanical milling (MM) is capable of producing nanocrystalline, nanosized, nanostructured, amorphous and metastable crystalline alloys. Since MM, specifically utilized to obtain nanomaterials, is based on sequential welding, fracturing and re-welding of the materials due to the kinetic energy produced during collisions between the balls, there are plenty of imperfections generated during these collisions [1]. For the last two decades different MM routes have been developed so as to produce nanocrystalline particles. Mechanical alloying (MA) [6], mechanical alloying with annealing (MAA) [7], cryo-milling [8], and reactive milling or mechanochemistry (MC) [9], are among those newly developed methods. MC has a special place since it not only produces nanoparticles but also permits chemical reactions. Moreover, it is also possible to initiate solid–solid, solid–liquid and solid–gas reactions with MC [10–12].

Manganese ferrite, $MnFe_2O_4$, has an 80% normal spinel structure that means 20% of Mn^{2+} ions occupy octahedral sites along with Fe^{3+} ions [13]. Manganese ferrites have been used in applications in fields such as magnetic resonance imaging, biosensor, and hyperthermia [14–16]. There are various methods in the literature that were utilized for the synthesis of $MnFe_2O_4$ nanoparticles. Stoichiometric nanoparticles can be prepared by thermal decomposition [14], sol–gel [17], co-precipitation [18], micro-emulsion [19] and mechanical milling [20–26], etc.

It is seen that the number of studies in the literature on the synthesis of $MnFe_2O_4$ nanoparticles by mechanical milling is very limited. In most of the studies, besides

*Corresponding author.
Tel.: +90 312 297 72 29; fax: +90 312 299 30 37.
E-mail address: sadan@hacettepe.edu.tr (S. Ozcan).

0272-8842/$ - see front matter © 2013 Elsevier Ltd and Techna Group S.r.l. All rights reserved.
http://dx.doi.org/10.1016/j.ceramint.2012.12.039

utilizing oxides as the starting materials, there have been the needs for post-synthesis procedures such as annealing and washing. First recorded work on the synthesis of $MnFe_2O_4$ nanoparticles was performed by Ding et al. [16]. In this work, Mn_2O_3 and Fe_2O_3, powders were used as the starting materials and milling was performed for 66 h under argon atmosphere in order to complete the phase formation. Muroi et al. [21] have, in general, followed a procedure that used high-energy mechanical milling of $FeCl_3$ and MnO powders followed by post-annealing steps performed at temperatures in the range of 500–600 °C. Moreover, they had to wash the samples several times with deionized water to get rid of $MnCl_2$, $FeCl_3$ and MnO residues. Mahmoud et al. [22] simply milled $MnFe_2O_4$ bulk materials that were synthesized by solid-state reaction in order to investigate the effect of mechanical milling on the cation distribution in the $MnFe_2O_4$ nanoparticles. Padella and Alvani [23,24] have chosen MnO and Fe_2O_3 as the starting stoichiometric powder mixture for high-energy mechanical milling, and they were able to synthesize $MnFe_2O_4$ nanoparticles in a single step without using any annealing procedure. However, they obtained approximately 100 nm agglomerates of strained nanocrystals with an average particle size of 5 nm. As a different starting material, Osmokrovic et al. [25] have used $MnCO_3$ along with Fe_2O_3. They have observed that after 10 h milling $MnFe_2O_4$ phase formation starts and phase formation is completed after 20 h. Nevertheless, they still had to anneal the as-milled samples at 400 °C for 4 h to form nanocrystalline particles. Alternatively, Aslibeiki et al. [26] started from a powder mixture of Mn-nitrate, Fe-nitrate and citric acid with an equal molar ratio of metal nitrates to citric acid. However, they also, had to utilize post-annealing steps at various temperatures to obtain $MnFe_2O_4$ nanoparticles with different sizes.

In this work, as an alternative and different method than those available in the literature, we describe the wet milling synthesis of nanocrystalline $MnFe_2O_4$ in a single step process starting with metallic Fe and Mn powders in distilled water. In addition, the effects of dry milling and wet milling on the crystallite size and the magnetic properties of $MnFe_2O_4$ nanocrystalline samples have been investigated.

2. Experimental

Pure elemental powders of Mn (−325 mesh, 99%) and Fe (−100 mesh, 99%) were used as the starting materials. The powders were mixed within distilled water with a molar ratio of 1(Mn): 2(Fe): 4(H_2O) placed in a cylindrical 250 ml tungsten-carbide vial with 10 mm diameter tungsten-carbide balls. The mixture in the vial was prepared and sealed in a glove box under argon atmosphere in order to provide an inert environment for the mechanochemical reaction. The mechanical milling was carried out in a planetary ball mill (Retch PM100) with a ball-to-powder weight ratio of 40:1. In order to investigate the effect of milling time on the formation of $MnFe_2O_4$ phase and the crystallite size, the wet milling was performed for 12, 18, 24 and 36 h at 400 rpm labeled as W12h, W18h, W24h, W36h, respectively. For further size reduction, smallest crystallite size samples synthesized by wet milling have been dry milled for 2 and 4 h at 300 rpm and labeled as D2h and D4h, respectively.

X-ray diffraction (XRD), x-ray photoelectron spectroscopy (XPS), and transmission electron microscopy (TEM) were used to investigate the structural properties of the nanocrystalline powders. XRD measurements were performed using a Rigaku D-Max B horizontal diffractometer using CuK_α radiation $\lambda = 1.54205$ Å at a scanning rate of $0.02^\circ\ s^{-1}$, in a range of 2θ from 20° to 80°. Oxidation state of Mn and Fe in the samples was determined by XPS carried out in a Termo k-Alpha Spectrophotometer in order to confirm $MnFe_2O_4$ phase formation. Electron microscopy analysis was carried out in an FEI, Tecnai G2 F30 Model TEM operated at 300 kV. From the TEM images, average particle sizes were calculated by using ImageJ software. Using a Quantum Design Physical Property Measurement System (PPMS) system with a vibration sample magnetometer module, magnetization measurements were done as a function of magnetic field and temperature.

3. Results and discussion

The XRD patterns of wet milled samples are shown in Fig. 1. The XRD patterns of possible structures that might form during the milling process are also added to the figure to comparatively follow the $MnFe_2O_4$ phase formation with milling time. It is seen that after 12 h three different phases, namely Fe, MnO, Fe_2O_3, were formed. Manganese does not react with water under normal conditions. However, MM activates reactions via mechanical stresses [1] and Mn gets completely oxidized whereas Fe is partially

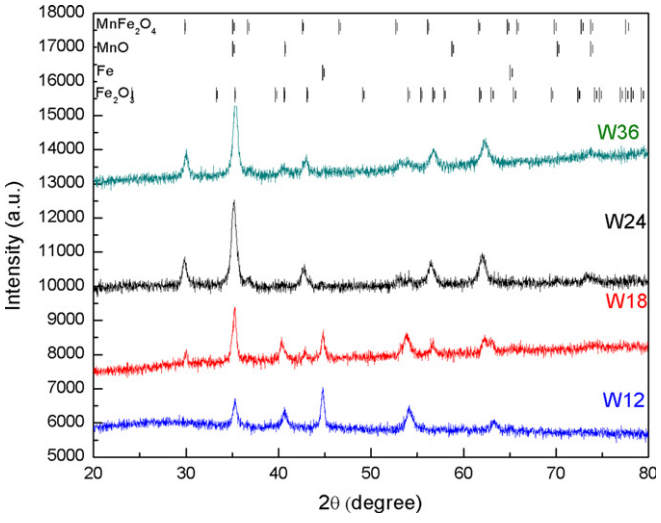

Fig. 1. XRD patterns of the wet milled samples milled for different milling time at constant milling speed.

converted to Fe_2O_3. On the other hand, no diffraction peaks of $MnFe_2O_4$ are observed. Although 18 h milling does not cause any significant change in the pattern, the relative intensity of Fe peaks reduces as an indication of further oxidation. One can easily check this fact by comparing Fe (110) peaks at $2\theta = 44.76^\circ$. However, increasing the milling time to 24 h creates a pronounced change in the structure. All of MnO, Fe and Fe_2O_3 turn to single phase $MnFe_2O_4$. The pattern of W24h perfectly matches with the standard pattern for the cubic spinel phase of $MnFe_2O_4$ (PDF#73-1964) and no characteristic peaks of any impurities are detected. On the other hand, increasing the milling time to 36 h leads to the deformation of target phase as well as increasing the crystallite size. This is an expected observation due to the deteriorating effects of thermal energy resulted by excessive milling [27,28]. According to the phase formation, a trend observed by XRD investigations, we deduce that $MnFe_2O_4$ by wet milling forms according to the following chemical reactions:

$$Mn + 2Fe + 2H_2O \rightarrow MnO + Fe_2O_3 + 2H_2$$

$$MnO + Fe_2O_3 + H_2 \rightarrow MnFe_2O_4 + H_2$$

which are not normally observed at room temperature. However, the first reaction initiates due to the impact energy that provides clean and fresh surfaces that are available for the oxidation of metallic Mn and Fe. It then leads to the formation of $MnFe_2O_4$.

Because of phase deformation and crystallite size increase, wet milling has been abandoned and dry milling has been implemented on the smallest crystallite size $MnFe_2O_4$ sample (W24h) obtained by wet milling. With the aim of avoiding the heating effect, dry milling was carried out at a low milling speed and time (300 rpm, 2 h and 4 h). In Fig. 2, XRD patterns of dry milled samples, D2h and D4h along with W24h are given. As can be seen from the Fig. 2, while the phase is intact, the (311) diffraction peak broadens which indicates size reduction.

In the literature, Scherrer equation that is based on the broadening of diffraction peaks is usually used for the calculation of crystal size from XRD patterns. However, it is very well known that strain has a pronounced effect on the broadening of diffraction peaks [29,30]. Since in mechanical milling strain is inevitable, one should consider this fact. Therefore, instead of Scherrer equation, it is more appropriate to utilize Williamson–Hall equation (Eq. (1)) [31,32], which includes both the effects of size and strain on the crystal:

$$\beta_{tot} = \beta_{crystal} + \beta_{strain} = 4\varepsilon \tan\theta + \frac{0.9\lambda}{D\cos\theta} \quad (1)$$

where β_{tot} is the full width at half maximum (in radians) of the XRD peaks, ε is the average strain, λ is the X-ray wavelength, θ is the peak positions and D is the crystal size.

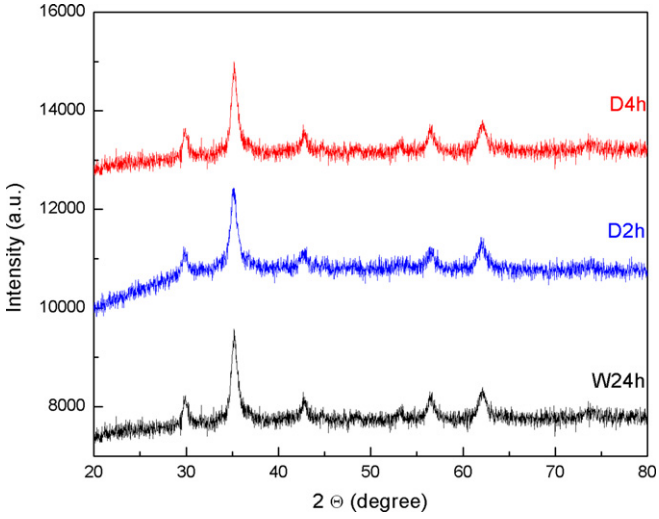

Fig. 2. XRD patterns of wet and dry milled nanocrystalline samples.

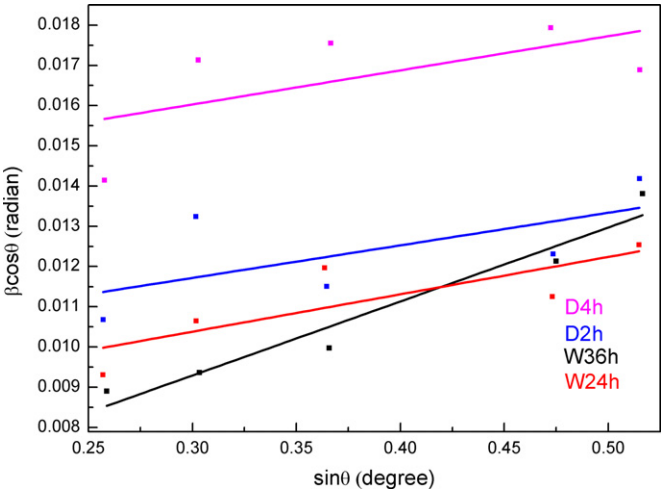

Fig. 3. Williamson–Hall plots of nanocrystalline $MnFe_2O_4$ samples.

By multiplying both sides with $\cos\theta$, one gets,

$$\beta_{tot}\cos\theta = 4\varepsilon \sin\theta + \frac{0.9\lambda}{D} \quad (2)$$

Therefore, by plotting versus $\sin\theta$, the strain component and crystal sizes are calculated from the slope and the intercept, respectively.

Fig. 3 shows Williamson–Hall plots of W24h, W36h, D2h, and D4h. From the figure it is clearly seen that intercept decreases to a lower value from W24h to W36h as the crystal size increases from 18.4 to 21.8 nm while intercept values progressively increase from W24h to D4h upon crystal size reduction, namely from 18.4 to 8.7 nm, by dry milling. When the strain components of the samples are compared, it is realized that wet milled sample, W36h possesses higher strain, 0.46% as opposed to dry milled samples, 0.20% where there is no visible slope change exist. It is well known that the strain in milled samples is due to the dislocations and other crystal defects [1]. Therefore, we infer that W36h sample acquires the

most defects and dislocations whereas dry milling decreases these defects, as it is inferred from the lower strain values provided in Table 1.

XPS spectrum of W24h given in Fig. 4 confirms the valance states of Mn and Fe for the single phase $MnFe_2O_4$. All the peaks reported were charge corrected with respect to C 1*s* peak position at 284.5 eV. Fig. 4 shows the high-resolution XPS spectra of the Fe 2*p* (a) and Mn 2*p* (b) photoelectron peak regions. $2p_{3/2}$ and $2p_{1/2}$ peaks appeared at 710.15 and 723.99 eV for Fe and 641.21 and 652.82 eV for Mn are consistent with the reported values for Fe^{3+} and Mn^{2+}, respectively [33,34].

Table 1
Crystallite, particle sizes and strain of the samples.

Sample	Crystallite size (nm)	Particle size (nm)	Strain (%)
W24h	18.4	19.6	0.23
W36h	21.8	–	0.46
D2h	12.4	–	0.20
D4h	8.7	27.9	0.20

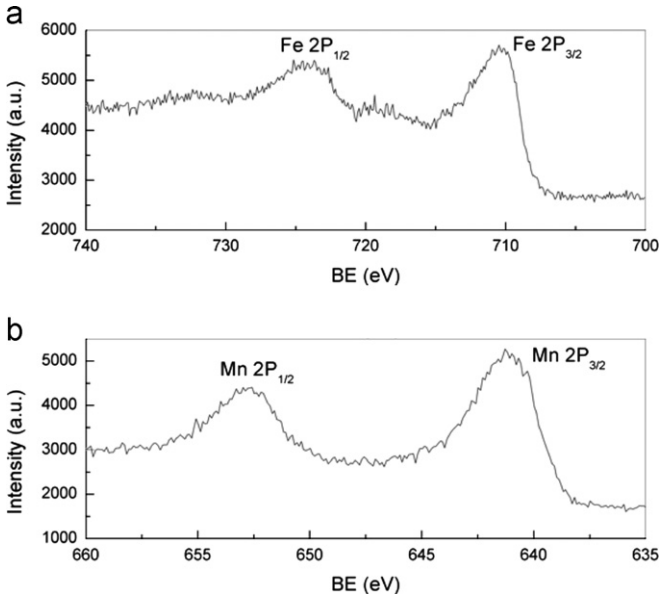

Fig. 4. XPS spectra for Fe (a) and Mn (b) regions of W24h.

TEM image of the samples W24h and D4h are given in Fig. 5. Overall, our observations reveal pronounced agglomeration of the particles, which is one of the main drawbacks of ball milling, nevertheless a roughly spherical morphology of the particles is distinguishable. Selected area diffraction (SAD) also shown in Fig. 5b as inset manifests the polycrystalline nature of the sample. The corresponding ring pattern of $MnFe_2O_4$ can be seen throughout the TEM sample which proves the uniformity of the $MnFe_2O_4$ structure in the sample. The inset given in Fig. 5a clearly shows the small spherical particles that could be separated via sonication as done for the TEM sample preparation.

From Fig. 5, average particle sizes of the samples W24h and D4h were calculated to be 19.6 and 27.9 nm, respectively, by using ImageJ software. The crystalline and particle sizes of W24 obtained from XRD and TEM, respectively are consistent. However, there is pronounced difference in the sizes (8.7 nm vs. 27.9 nm) obtained for D4h. These results could be attributed to the water used for wet milling acting as a lubricant preventing strong welding of the fractured particles. On the other hand in dry milling while welding effect is inevitable and leads to particle size increase, the crystallite size becomes smaller. Similar results were reported by Meng et al. and Zhou et al. [35,36].

In order to investigate the effect of crystallite size and average particle size on magnetic properties, temperature (*M–T*) and field dependent magnetization (*M–H*) measurements were carried out. Field dependent magnetization measurements at 300 and 5 K on samples W24, D2 and D4 are plotted in Fig. 6. The insets of the figures show magnified region around the zero field to make it more visible. Since all the samples clearly show hysteresis, it is understood that the samples are

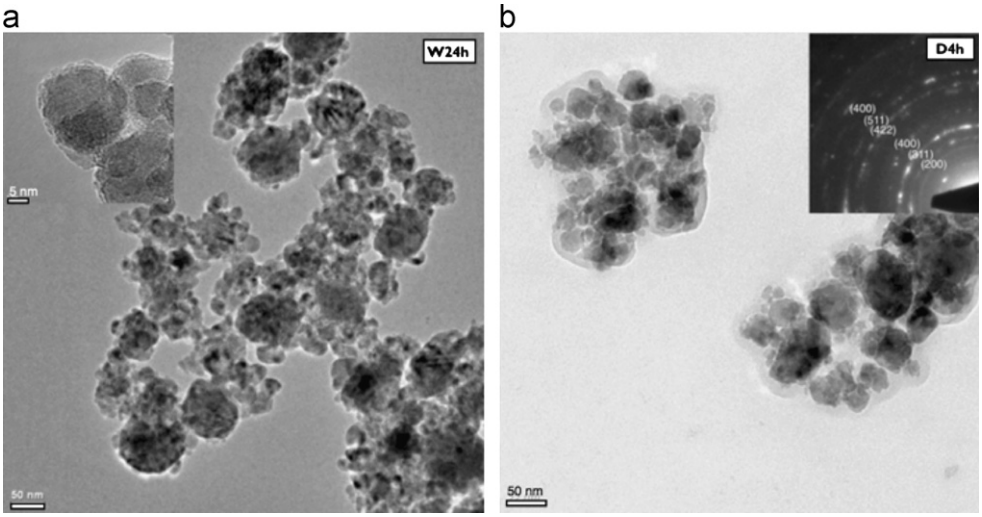

Fig. 5. TEM images of W24h (a) and D4h (b). Insets: HRTEM image of W24h (a) and SAD pattern of D4h (b).

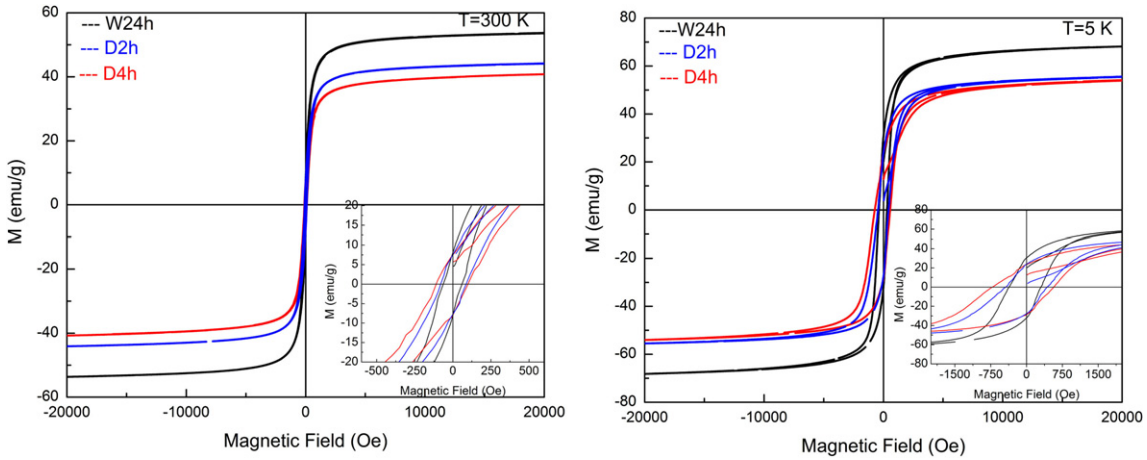

Fig. 6. *M–H* loops of nanocrystalline $MnFe_2O_4$ at 300 K (left) and 5 K (right).

ferromagnetic. The most prominent observation obtained by *M–H* measurements is the reduction of 2 T magnetization values. Generally, it is known that decreasing particle size leads to decreasing saturation magnetization. However, one notices that two different particle size samples W24h and D4h behave different. Lower particle size W24h acquires magnetization at 2 T as compared to D4h. Therefore, we infer that the crystalline size has more effect on the magnetic properties than particle size. Although particle size increases, the crystallite size decreases and this, in turn, results in a structure with larger magnetically dead layer and stoichiometric deviations around the grain boundary. These are, however, natural results of mechanical milling.

Room temperature magnetization values for these samples are 53.72, 44.10, and 40.70 emu/g, respectively. These values are smaller than those of bulk $MnFe_2O_4$. Similar observations have been obtained by Aslibeiki et al. [26]. Even though crystallite sizes are small, even a large field of 2 T is not able to saturate the magnetization due to strong local anisotropic changes. Similarly, *M–H* curves possess traces of those effects at 5 K. Magnetization values increase relative to 300 K values due to the reduction of randomizing effect of temperature and the value of magnetizations at 2 T are 68.12, 55.52 and 54.08 emu/g for samples W24h, D2h and D4h, respectively. Similar values are reported in different studies for comparable size $MnFe_2O_4$ nanoparticles [21,37].

Another important observation is that although the crystallite size of the samples is well below the superparamagnetic limit of $MnFe_2O_4$, field dependent magnetization curves at 300 K and 5 K possess coercivity. Critical size for superparamagnetic behavior for $MnFe_2O_4$ is known to be approximately 50 nm. The crystallite size obtained by structural investigation is below this limit. Variation of the magnetization with external field at room temperature exhibits coercivities of 72.88, 80.31 and 115.37 Oe for the samples W24h, D2h and D4H, respectively. This is attributed to magnetic interactions between the agglomerated particles as well as large particle size

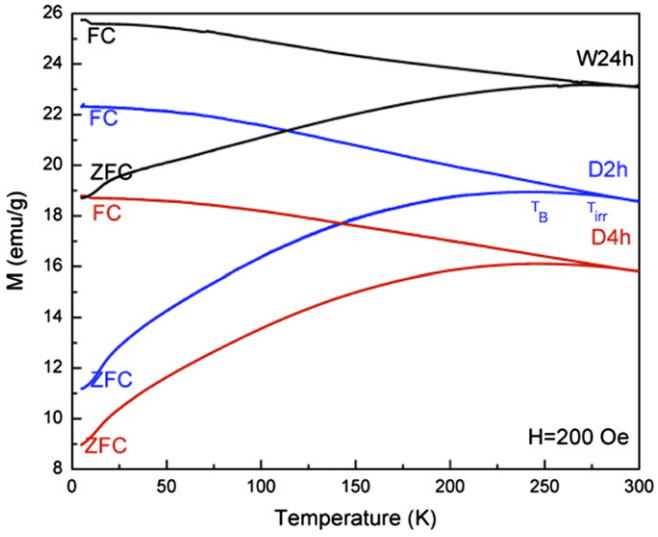

Fig. 7. Temperature dependence of field cooled and zero field cooled magnetizations of nanocrystalline $MnFe_2O_4$.

distribution realized by TEM observations. Reduction of temperature affects coercivity of the samples as well. Consistently, coercivity increases with temperature. With the reduction of temperature, coercivities of W24h, D2h and D4h become 365.21, 441.34 and 723.05 Oe, respectively, at 5 K. In the literature, another way to determine the magnetic interaction is comparing the M_r/M_s ratio. If M_r/M_s is equal to 0.5, the nanoparticles are non-interacting Stefan Wolfhard superparamagnetic particles. If M_r/M_s is less 0.5, then the nanoparticles possess magnetetostatic interactions [38]. For our three samples M_r/M_s is about 0.4 indicating that our samples are interacting, as expected.

Temperature dependence of the magnetization shown in Fig. 7 was investigated by zero field cooled (ZFC) and field cooled (FC) measurements using 200 Oe applied field. Splitting of FC–ZFC curves is known as the irreversibility temperature T_{irr} corresponding to the particles with the highest energy barrier while the peak

temperature of the ZFC curve is defined as the blocking temperature, T_B. Although T_{irr} point does not seem to change with crystallite size and remains around 280 K, it is noticed that as expected T_B shifts to lower temperatures with decreasing crystallite size. In addition, the large humps of ZFC curves are consistent with broad size distribution observed by TEM images.

4. Conclusions

Nanocrystalline $MnFe_2O_4$ particles were synthesized from metallic Mn and Fe powders in the single step wet milling process. Formation of single phase nanocrystalline $MnFe_2O_4$ particles was confirmed by structural and magnetic investigations yielding consistent results with the literature. Structural and magnetic properties of wet milled samples were compared with dry milled samples. It was found that crystalline size increased by further wet milling after nanocrystalline $MnFe_2O_4$ is obtained. However dry milling utilized for size reduction lead to lower crystalline size but higher particle size. This effect manifested itself on the magnetic properties as well. High particle size with low crystal size sample (D4h) showed lower magnetization as compared to low particle size high crystal size sample (W24h). Therefore, wet milling followed by a dry milling step, if needed, is suggested as an alternative and simple route for the production of nanocrystalline $MnFe_2O_4$.

Acknowledgment

This work is supported by Hacettepe University, Scientific Research and Development Office, through the Grant no. 0901602001.

References

[1] C. Suryanarayana, Mechanical Alloying and Milling, Marcel Dekker, New York, 2004.
[2] S. Berger, R. Porat, R. Rosen, Nanocrystalline materials: a study of WC-based hard metals, Progress in Materials Science 42 (1997) 311–320.
[3] J. Chicinas, Soft magnetic nanocrystalline powders produced by mechanical alloying routes, Journal of Optoelectronics and Advanced Materials 8 (2006) 439–448.
[4] H. Gleiter, Nanostructured material: basic concepts and microstructure, Acta Materialia 48 (2000) 1–29.
[5] S.L. Malgorzata, High-Energy Ball Milling Mechanochemical Processing of Nanopowders, Boca Raton, Boston, New York Washington, DC, 2010.
[6] Z. Pengfei, et al., Physical and surface characteristics of the mechanically alloyed, SiBCN powder, Ceramic International 38 (8) (2012) 6399–6404.
[7] S. Ozcan, B. Kaynar, M.M. Can, T. Firat, Materials Science and Engineering B 121 (2005) 278–281.
[8] C.S. Tiwary, et al., Preparation of ultrafine CsCl crystallites by combined cryogenic and room temperature ball milling, Ceramic International 37 (8) (2011) 3677–3686.
[9] M.M. Can, S. Ozcan, A. Ceylan, T. Firat, Effect of milling time on the synthesis of magnetite nanoparticles by wet milling, Materials Science and Engineering B 172 (2010) 72–75.
[10] I. Ismail, M. Hashim, K.A. Matori, R. Alias, J. Hassan, Dependence of magnetic properties and microstructure of mechanically alloyed $Ni_{0.3}Zn_{0.7}Fe_2O_4$ on soaking time, Journal of Magnetism and Magnetic Materials 323 (2012) 1470–1476.
[11] S. Ozcan, M.M. Can, A. Ceylan, Single step synthesis of nanocrystalline ZnO via wet-milling, Materials Letters 64 (2010) 2447–2449.
[12] M.Y. Song, S.H. Kwan, S.H. Hong, H.R. Park, Hydrogen storage properties of a Ni, Fe and Ti-added Mg-based alloy, Metals and Materials International 18 (2012) 279–286.
[13] S. Chikazumi, Physics of Ferromagnetism, 2nd ed., Oxford University Press Inc., New York, 1997.
[14] H. Yang, et al., Water-soluble superparamagnetic manganese ferrite nanoparticles for magnetic resonance imaging, Biomaterials 31 (2010) 3667–3673.
[15] S.G. Grancharov, et al., Biofunctionalization of monodisperse magnetic nanoparticles and their use as biomolecular labels in a magnetic tunnel junction based sensor, The Journal of Physical Chemistry B 109 (2005) 13030–13035.
[16] P. Pradhan, J. Giri, R. Banerjee, J. Bellare, D. Bahadur, Cellular interactions of lauric acid and dextran coated magnetite nanoparticles, Journal of Magnetism and Magnetic Materials 311 (2007) 208–215.
[17] X. Hou, J. Feng, Y. Ren, Z. Fan, M. Zhang, Synthesis and adsorption properties of spongelike porous $MnFe_2O_4$, Colloids and Surfaces A: Physicochemical and Engineering Aspects 363 (2010) 1–7.
[18] V. Musat, et al., Magnetic materials from co-precipitated ferrite nanoparticles, Materials Science and Engineering B 167 (2010) 85–90.
[19] M. Bellusci, et al., Phase evolution in synthesis of manganese ferrite nanoparticles, Journal of the American Ceramic Society 90 (2007) 3977–3983.
[20] J. Ding, P.G. McCormick, R. Street, Formation of spinel Mn-ferrite during mechanical alloying, Journal of Magnetism and Magnetic Materials 17 (1997) 309–314.
[21] M. Mouri, R. Street, P.G. McCormick, J. Amighian, Magnetic properties of ultrafine $MnFe_2O_4$ powders prepared by mechanochemical processing, Physical Review B 63 (2001) 184414–184420.
[22] M.H. Mahmoud, H.H. Hamdeh, A.I. Abdel-Mageed, A.M. Abdallah, M.K. Fayek, Effect of HEBM on the cation distribution of Mn-ferrite, Physica B: Condensed Matter 291 (2000) 49–53.
[23] F. Padella, C. Alvani, A. La Barbera, G. Ennas, R. Liberatore, F. Varsano, Mechanosynthesis and process characterization of nanostructured manganese ferrite, Materials Chemistry and Physics 90 (2005) 172–177.
[24] C. Alvani, G. Ennas, A. La Barbera, G. Marongiu, F. Padella, F. Varsano, Synthesis and characterization of nanocrystalline $MnFe_2O_4$: advances in thermochemical water splitting, International Journal of Hydrogen Energy 30 (2005) 1407–1411.
[25] P. Osmokrovic, C. Jovalekic, D. Manojlovic, M.B. Pavlociv, Synthesis of $MnFe_2O_4$ nanoparticles by mechano-chemical reaction, Journal of Optoelectronics and Advanced Materials 8 (2006) 312–314.
[26] B. Aslibeiki, P. Kameli, H. Salamati, M. Eshraghi, T. Tahmasebi, Superspin glass state in $MnFe_2O_4$ nanoparticles, Magnetism and Magnetic Materials 322 (2010) 2929–2934.
[27] C. Kuhrt, H. Schropf, L. Schultz, E. Arzt, Mechanical Alloying for Structural Applications, ASM International, Materials Park, OH, 1993, pp. 269–273.
[28] A.N. Straleski, et al., Amorphization and reactivity of silicon induced by mechanical treatment, Materials Science Forum 386–388 (2002) 187–192.
[29] I. Lucks, P. Lamparter, J. Xu, E.J. Mittemeijer, X.R.D. Line, Broadening analysis with ball milled Palladium, Materials Science Forum 443–444 (2004) 119–122.
[30] I. Lucks, P. Lamparter, E.J. Mittemeijer, An evaluation of methods of diffraction-line broadening analysis applied to ball-milled molybdenum, Journal of Applied Crystallography 37 (2000) 300–303.

[31] B.D. Cullity, S.R. Stock, Introduction to Magnetism and Magnetic Materials, 3rd ed., Prentice Hall, Upper Saddle River, NJ, 2002.
[32] P. Kameli, H. Salamati, A. Aezami, Effect of particle size on the structural and magnetic properties of $La_{0.8}Sr_{0.2}MnO_3$, Journal of Applied Physics 100 (2006) 053914–053920.
[33] I. Bilecka, M. Kubli, E. Amstad, Simultaneous formation of ferrite nanocrystals and deposition?of thin films via a microwave-assisted nonaqueous sol–gel process, Journal of Sol–Gel Science and Technology 57 (2011) 313–322.
[34] G. Leem, et al., Light-induced covalent immobilization of monolayers of magnetic nanoparticles on hydrogen-terminated silicon, Applied Materials Interfaces 2 (2010) 2789–2796.
[35] L. Meng, Improved Hydrogen Sorption Kinetics in Wet Ball Milled Mg hydrides, Energy & Environment, 93 Forschungszentrum Jülich GmbH, 2010.
[36] P.H. Zhou, et al., A study about Fe–Ni mechanical alloying process by dry and wet method, Journal of Electronic Science and Technology of China 2 (2005) 164–167.
[37] C. Liu, J. Zhang, Size-dependent superparamagnetic properties of Mn spinel ferrite nanoparticles synthesized from reverse micelles, Chemistry of Materials: A Publication of the American Chemical Society 13 (2001) 2092–2096.
[38] A. Tamion, M. Hillenkamp, F. Tournus, E. Bonet, V. Dupuis, Accurate determination of the magnetic anisotropy in cluster-assembled nanostructures, Applied Physics Letters 95 (2009) 1–3.